Applied Catalysis B: Environmental 174–175 (2015) 244–252

Contents lists available at ScienceDirect

Applied Catalysis B: Environmental

journal homepage: www.elsevier.com/locate/apcatb

Preparation, characterization and photocatalytic performance of pyrolytic-tire-char/TiO_2 composites, toward phenol oxidation in aqueous solutions

V. Makrigianni, A. Giannakas, C. Daikopoulos, Y. Deligiannakis, I. Konstantinou*

Department of Environmental and Natural Resources Management, University of Patras, G. Seferi 2, Agrinio 30100, Greece

ARTICLE INFO

Article history:
Received 17 November 2014
Received in revised form 26 February 2015
Accepted 5 March 2015
Available online 7 March 2015

Keywords:
Pyrolytic char
TiO_2
Photocatalysis
Phenol
EPR

ABSTRACT

A pyrolytic char/TiO_2 (PC/TiO_2) composite material, where PC was derived from recycled tires, was prepared by the sol–gel method. XRD analysis showed formation of TiO_2 anatase phase, as well as, a small fraction of brookite phase. UV–vis DRS spectroscopy showed that PC/TiO_2 composites have enhanced absorption at visible wavelengths 340–450 nm. The photocatalytic activity and the promoting effect of PC/TiO_2 composite catalysts were investigated for the degradation of phenol in aqueous suspensions. The photocatalytic degradation followed pseudo-first order kinetics. The ratio TiO_2:PC (w:w) largely affected the performance of the composite catalysts. The optimal (w:w = 0.1) ratio was found e.g., (0.2 g PC, 2 g TiO_2). An important finding is a significant promoting effect of PC on the photocatalytic performance of TiO_2. Electron paramagnetic resonance (EPR) spectroscopy showed that the pyrolytic char acts as a very efficient electron-acceptor from TiO_2 particles under UV–vis irradiation. This resulted in decreased electron–hole pair recombination and subsequently in enhanced production of OH-radicals that oxidized phenol. Thus, PC matrix can act as an electron storage matrix for photo-induced electrons from TiO_2.

1. Introduction

Heterogeneous photocatalysis has been proposed as an environmental efficient method for purifying water and air [1,2]. Titanium oxide (TiO_2) is widely used as photocatalyst for removing pollutants from water because of its low cost, high chemical stability and unique electronic and optical properties [3,4]. However, its photocatalytic activity is hindered by its wide band gap (3.0–3.2 eV) which is activated only under ultraviolet (UV) light irradiation, and by competing hole–electron (h^+–e^-) recombination. Several methods have been proposed to improve the photocatalytic activity of TiO_2, e.g., narrowing the semiconductor's bang-gap by doping TiO_2 with transition metals (Au, Pt, Rh, etc.), doping TiO_2 with nonmetals (N, S, F, etc.) or via co-doping methods (N—S, N—F, N—I) [5,6]. In addition, it has been demonstrated that the rate of photodegradation of pollutants by TiO_2 is enhanced by loading TiO_2 onto adsorbents with high pollutant adsorption capability [7–11].

Activated carbon (AC), as a support for TiO_2, is the most common type of adsorbent that has been used in the photodegradation of organic pollutants in aqueous phase, that has been shown to promote the catalytic efficiency of TiO_2 [12–16]. The enhancement is attributed to the so-called synergistic effect e.g., the adsorbent may adsorb a large amount of pollutant, thus, facilitating the proximity/reaction of pollutant with the TiO_2 surface, where the photocatalytic degradation of pollutant takes place. Although AC has typically large surface area and high adsorption capacity, the presence of micropores in activated carbon hinders the diffusion of adsorbed pollutant toward the TiO_2 surface, while the deposition of TiO_2 may block the micropores of AC and thus, reduce its surface area [18].

Pyrolytic char from tire-rubber and other industrial or agricultural by-products, a newest type of adsorbent similar to carbon black (CB), was chosen as another support in order to improve the photo-efficiency of TiO_2 [17–19]. Pyrolysis involves the decomposition of the tire-rubber at high temperatures in oxygen-free atmosphere. This process presents an alternative to scrap tire disposal which results in the recovery of valuable products, oil and gas fractions, plus the pyrolytic char (PC) [20]. Rincon et al. [21] showed that the enhancement of photocatalytic activity of the TiO_2/carbon black composite catalysts is mainly due to the role of carbon on hole–electron photogeneration and transport. So far, most photocatalytic studies on carbon-TiO_2 composite materials have been carried out with TiO_2/AC, however, some studies [18,19] reveal that nanocomposite photocatalysts (carbon black/TiO_2)

* Corresponding author. Tel.: +30 2641074186; fax: +30 26410 74176.
E-mail address: iokonst@upatras.gr (I. Konstantinou).

http://dx.doi.org/10.1016/j.apcatb.2015.03.007
0926-3373/

prepared by the sol–gel method, exhibited higher photocatalytic activity compared to TiO_2/AC composite catalysts [22,23] prepared with the same method. It has been proven that carbon black possess a well-developed mesoporous structure that results in relatively high adsorption capacities for organic pollutants, as well as, high electrical conductivity which can reduce the photo-induced electron–hole recombination rate in TiO_2 [18,19]. Due to the above-mentioned characteristics, a better synergy effect can be observed when TiO_2 incorporated on carbon black in the photocatalytic degradation of organic pollutants. However, so far pyrolytic chars, a carbonaceous support that present similar properties to carbon black, have never been tested in TiO_2 composite photocatalysts.

In the present work, we report the preparation of tire-char/TiO_2 composite catalysts (PC/TiO_2) by a sol–gel impregnation method under various char content (wt. %) ratios. The as-prepared catalysts were characterized by XRD, IR spectroscopy, N_2-porosimetry and ultra violet–visible diffuse reflectance spectroscopy (UV–vis DRS). In addition, electron paramagnetic resonance spectroscopy (EPR) has been used to [i] detect the photo-induced holes (h^+)–electrons (e^-) in the composite catalysts, [ii] probe the photogenerated •OH radicals in solution. The photocatalytic performance of the PC/TiO_2 catalysts has been assessed for the photooxidation of phenol aqueous solutions in order to evaluate the possible synergistic effect of PC/TiO_2 composite catalysts and optimize the (wt. %) char/TiO_2 ratio.

2. Experimental

2.1. Preparation of pyrolytic char/TiO_2 (PC/TiO_2) composites

The char was derived from the pyrolysis of used rubber tires at 450 °C in oxygen-free atmosphere under vacuum for 4 h. The as-received pyrolytic char (PC) was initially purified as follows: 10 g of char was suspended in 1 L of HNO_3 2 N solution and was left for 24 h under vigorous stirring. The suspension was filtered and the PC powder was refluxed with 200 mL HNO_3 2 N solution for 48 h, according to previous report [24]. For the preparation of PC/TiO_2 composite, 6.8 mL tetrabutylorthotitanate (TBOT) was added drop wise to 50 mL of Milli-Q grade water and the solution was stirred for 12 h at 25 °C in order to complete the hydrolysis. Then, the appropriate amount of char (0.1, 0.2, 0.5, 0.7 and 1.0 g) was added and the black sol was left for 12 h under stirring. The resulted suspension was spread into Petri dish and dried for 24 h at 110 °C under ambient air. The resulted xerogels were calcined for 1 h at 500 °C to obtain the final char/TiO_2 nanocomposites. For the preparation of blank TiO_2 sample, the same procedure was repeated without the addition of char. In addition, a blank char sample was prepared without addition of TBOT with the same 'procedure, and labeled as Char500. Herein, the obtained materials were code-named by their total weight ratio of Char (C) to Ti (T) used as follows: CT0.1/2, CT0.2/2, CT0.5/2, CT/0.7/2, CT1/2, Char500 and TiO_2-blank.

2.2. Morphology and surface area analysis

The crystal phases of all prepared PC/TiO_2 catalysts were characterized by recording their X-ray diffraction (XRD) patterns using a Brüker Advance D8 instrument employing Cu K radiation (λ = 1.5418 Å) in the 2θ range from 10° to 80° with a 2θ resolution of 0.02°. The XRD patterns were assigned using the Joint Committee on Powder Diffraction Standards (JCPDS) database and then were analyzed with Rietveld refinement using an applicable computer program. Crystal size was calculated by the well-known Sheerer's equation: $d = 0.9\lambda/b\cos\theta$, where d is diameter of crystallites in nm, λ the wavelength (nm) of the monochromatic X-ray beam, θ is the Bragg angle in degrees, and b is the FWHM. The results obtained from XRD analysis are presented in Fig. 1 and Table 1.

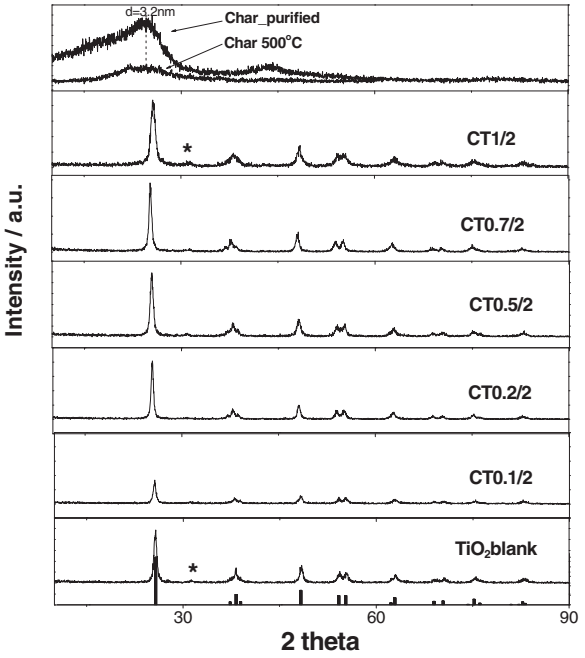

Fig. 1. XRD patterns for composite catalysts PC/TiO_2, pure TiO_2 blank, purified char and Char500. The bar graph in the bottom corresponds to anatase crystal phase reflections. * Signalizes (101) brookite reflection.

The morphology of the catalysts was studied using a JEOL JSM 6510 LV scanning electron microscope (SEM) coupled to xx-Act Energy Dispersive Spectrometer (EDS) from Oxford Instruments.

Nitrogen adsorption–desorption isotherms were determined at 77 K using a Tristar Micrometrics Instruments and the specific surface area of the char/TiO_2 composites was derived using the Brunauer–Emmett–Teller (BET) method. Specific surface area value for all PC/TiO_2 solids, TiO_2 blank and Char500 are included in Table 1.

2.3. Surface chemistry

The surface chemistry of PC-composites was analyzed by FT-IR spectroscopy and their point of zero charge (pH_{pzc}) [25]. FT-IR

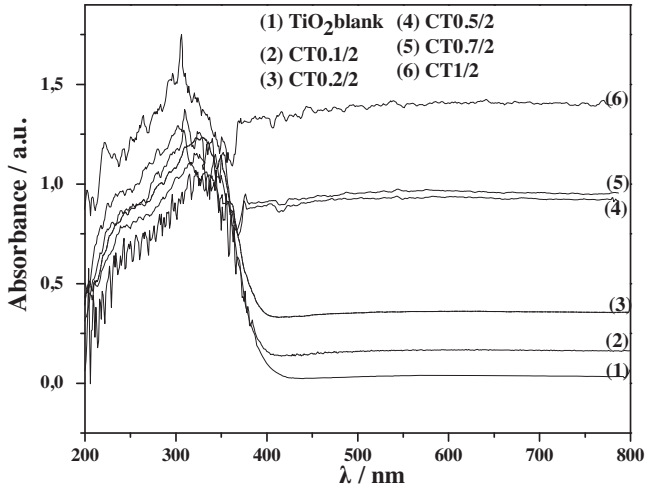

Fig. 2. UV–vis diffuse reflectance spectra of the PC/TiO_2 nanocomposites with different weight ratios and blank TiO_2.

Table 1
Results of XRD, Rietveld analysis, specific surface areas (BET), point zero of charge (pH_{pzc}), and band gap energies (E_g) for the nanocomposites PC/TiO_2 catalysts.

Catalyst code name	Crystal phase-space group	% Crystal phase detection	Rietveld analysis			Particle size d (nm)	BET (m^2/g)	pH_{pzc}	E_g
			a	b	c				
TiO_2 blank	Anatase- tetragonal 141	96	3.791	3.791	9.517	19	95	6.5	3.21
	Brookite-orthrombic *Pcba*	4	9.277	5.367	5.079	21			
Char500	Graphite *P63mc*	100	–	–	–	–	135	6.7	
CT0.1/2	Anatase- tetragonal 141	100	3.790	3.790	9.512	19	44.0	6.5	3.22
CT0.2/2	Anatase- tetragonal 141	100	3.788	3.788	9.513	18	61.3	6.2	3.23
CT0.5/2	Anatase- tetragonal 141	100	3.788	3.788	9.508	17	81.50	5.9	3.24
CT0.7/2	Anatase- tetragonal 141	100	3.787	3.787	9.514	17	78.45	5.8	3.19
CT1.0/2	Anatase- tetragonal 141	90	3.782	3.782	9.491	13	127.20	4.0	3.23
	Brookite- orthrombic *Pcba*	10	9.277	5.367	5.079	18			

of materials was recorded on a Spectrum GX PerkinElmer FT-IR System. The KBr pellets were prepared by mixing 2 mg of PC/TiO_2 with 20 mg KBr. It is stressed that low-percentage of materials PC/TiO_2:KBr has to be used in order to avoid distortion of certain bands.

The point of zero charge (pH_{pzc}) of PC/TiO_2 composite catalysts was determined by the potentiometric mass titration (PMT) technique. Prior to experimentation, a stock solution of 0.03 M KNO_3 electrolyte in ultrapure water was prepared under N_2 atmosphere. Mass titrations were performed for four aqueous suspensions with % weight ratios 0.01, 0.1, 1 and 5, at constant ionic strength and temperature (25 °C). During the titration, the aqueous suspensions were maintained under strong stirring with 600 rpm for 20 h in order to reach an equilibrium pH value. The pzc is easily determined from the appearance of a plateau in the curve "pH vs mass" [25,26]. The measured pH_{pzc} values for PC/TiO_2 catalysts are listed in Table 1.

2.4. UV–vis DRS measurements

The ultraviolet–visible diffuse reflectance spectra (UV–vis DRS) of the catalysts were measured by a PerkinElmer (Lamda 35) spectrophotometer equipped with an integrating sphere assembly, using $BaSO_4$ as the reflectance standard, at room temperature, in the wavelength range of 220–800 nm. The UV–vis DRS of all samples are shown in Fig. 2.

2.5. Elemental analysis

The elemental analyzer PerkinElmer (2400 Series II) was used to determine the carbon, hydrogen, nitrogen and sulfur (CHNS) contents of the samples. Oxygen content was determined by mass difference.

2.6. EPR experiments

Electron paramagnetic resonance (EPR) spectra were recorded at 77 K with a Brüker ER200D spectrometer, equipped with an Agilent 5310A frequency counter operating at the X band. Adequate signal to noise was obtained after 10–15 scans. The spectrometer was running under a home-made software based on lab view [27]. A solar-light-simulating Xe light source (Oriel model 66929, 450 W, $\lambda > 240$ nm) equipped with a water IR cut-off filter was used to monitor in situ inside the EPR cavity, the photo-generation of electrons (e^-) and holes (h^+). EPR samples were prepared by placing 10 mg of each PC/TiO_2 material into a quartz EPR tube (Suprasil, Willmad Glass) with an outer diameter of 3 mm.

The generation of hydroxyl (•OH) radicals produced by continuous irradiation ($\lambda > 240$ nm) of aqueous PC/TiO_2 suspensions, were determined by EPR using 5,5-dimethyl-1-pyrroline-*N*-oxide (DMPO) as a spin trap [28]. In each experiment, 6 mg of each PC/TiO_2 sample were dispersed in 10 ml of Milli-Q water (0.6 g L^{-1}). The pH was adjusted to 3.8 with HNO_3 solution and the suspension was placed in a water-bath sonicator for 20–30 min. Subsequently, the suspension was placed on a magnetic stirrer and 100 μL were transferred to 900 μL of Milli-Q water (0.06 g L^{-1}). The so-diluted suspension was sonicated for at least 15 min. In the resulting suspension 50 μL of freshly prepared DMPO (50 mM in water) solution was added (resulting in a concentration of 2.5 mM). 5,5-Dimethyl-1-pyrroline-*N*-oxide was purchased from Aldrich. Kinetic runs were performed in 2 capillaries containing 12 μL each, by recording the signal intensity of the DMPO-OH spectrum as a function of irradiation time at room temperature (25 °C). Spin quantitation was done using DPPH as a spin standard [29].

Our photoreaction setup was calibrated using P25 (TiO_2). According to detailed experiments, our setup produces 100 μmol •OH per gram of P25 (see Fig. 1S, Supplementary information) which is in very good agreement with literature [30].

2.7. Adsorption studies

Adsorption experiments were conducted using a batch equilibrium technique at 25 ± 1 °C in 250 mL sealed glass conical flasks containing 50 mL of phenol solution at different initial concentrations (C_0 in the range 2–100 mg L^{-1}) and 5 mg of each material. The suspensions were kept under dark and stirred at 600 rpm. The pH at the end of adsorption experiments was 6.5 ± 0.1. After reaching equilibrium, aliquots of the suspensions (≈2 mL) were filtered through a 0.45 μm filter (HVLP, Millipore) to separate the solid materials. Adsorption kinetics studies were carried out using conical flasks contained 100 mL of phenol solution at initial concentration (C_o = 10 mg L^{-1}) and 10 mg of each material. The suspensions were kept under dark and were stirred at 600 rpm. After reaching equilibrium at 60 min, aliquots of the suspension (≈2 mL) were filtered through a 0.45 μm filter (HVLP, Millipore) to separate the solid materials.

2.8. Photocatalytic oxidation of phenol

The irradiation of phenol/catalysts suspensions was carried out using a Suntest XLS + apparatus (Atlas, Germany) simulating natural sunlight irradiation. The light source was an air-cooled xenon lamp (2.2 kW) jacked with special glass filters restricting the transmission of wavelengths below 290 nm. An average irradiation intensity of 500 W m^{-2} was maintained throughout the experiments. Irradiation experiments were performed using a 250 mL cylindrical Pyrex glass UV-reactor equipped with a water-circulating circuit containing 200 mL of aqueous solutions. In addition, Suntest apparatus is equipped with a black standard thermometer (BST) to regulate air temperature conditions in the exposure chamber by air-cooling circuit. The irradiation was measured by a calibrated internal radiometer of the Suntest apparatus. The solution was mixed with the appropriate amount of catalyst and the suspension was magnetically stirred at 600 rpm before

and during the illumination. The suspension was kept in the dark for 60 min prior to illumination to reach adsorption equilibrium onto semiconductor surface. Irradiation experiments were performed using an initial concentration of phenol (C_o = 10 mg L^{-1}) and TiO_2 catalyst (C_o = 100 mg L^{-1}). As the reaction progressed, aliquots (≈2 mL) were withdrawn from the reactor at specific time intervals and filtered through a 0.45 μm filter (HVLP, Millipore) in order to remove the particles of catalyst.

2.9. Chromatographic analysis

Phenol concentrations were determined by a Dionex P680HPLC instrument equipped with a Dionex PDA-100 Photodiode Array Detector and a Discovery C18 (250 mm length × 4.6 mm ID: 5 μm particle size) column (Supelco, PA, USA). The mobile phase was a mixture of LC-grade water at pH 3 (50%) and acetonitrile (50%) with a flow rate of 1 mL min^{-1}. Column temperature was set at 40 °C. The detection of phenol was realized at 265 nm.

3. Results and discussion

3.1. XRD and SEM characterization

Fig. 1 shows the XRD patterns for the prepared PC/TiO_2 composites with different PC/TiO_2 weight ratios. A graphite-type, partially ordered phase was obtained in the case of pyrolytic char calcined at 500 °C. The reflections of TiO_2 tetragonal anatase phase, with tetragonal 141 space groups, for all composite catalysts according to the JCPDS-databank are included in the Fig. 1 (bottom bars). Also, traces of brookite crystal phase, with orthorhombic *Pcba* space group, was formed in both TiO_2 blank (≅4%) and CT 1/2 (≅10%) i.e., the composite with the highest char amount. Using the so-obtained phase for each solid as starting model, a Rietveld refinement of the XRD data was performed based on the methodology according to Ref. [31]. The refinement parameters including the cell parameters (a–c), crystal size and % crystal phase are presented in Table 1. The average particle size is calculated using Scherrer's equation [31]. The cell parameters (Table 1) for all PC composite catalysts show small differences, in comparison to the values of blank TiO_2 anatase phase.

The particle size of the composite catalysts is also important for the photocatalytic efficiency. The average particle size of anatase TiO_2 ($d_{anatase}$) ranged from 13 to 20 nm, while the average particle size of pure anatase phase was smaller than a simple mixture of anatase-brookite (Table 1). As shown in Fig. 1, the diffraction peak intensity of TiO_2 increases for larger size particles. Broader XRD pattern was observed in the case of CT 1/2, the composite with the highest amount of char, which correspond to the lowest particle size. It can be inferred that the presence of char surface suppresses the crystallite growth or inhibits the aggregation of TiO_2 hence, the particle size of TiO_2 reduces. A similar trend was previously reported for carbon black/TiO_2 [18] and activated carbon/TiO_2 composites [32].

In conclusion, the present XRD data demonstrate that (i) all composite PC/TiO_2 catalysts showed well crystalized TiO_2 nanoparticles, (ii) all composite catalysts mainly contained the anatase crystal phase (minor fractions of brookite phase were detected in CT 1/2), (iii) an increment of PC/TiO_2 ratio decreases the TiO_2 particle size.

SEM images of the char500 and CT0.2/2 samples are shown in Fig. 3a and b, respectively. Fig. 3b indicates immobilization of TiO2 agglomerates on the surface of char as well as the presence of a free carbonaceous surface. TiO_2 particles were well-dispersed on the char matrix.

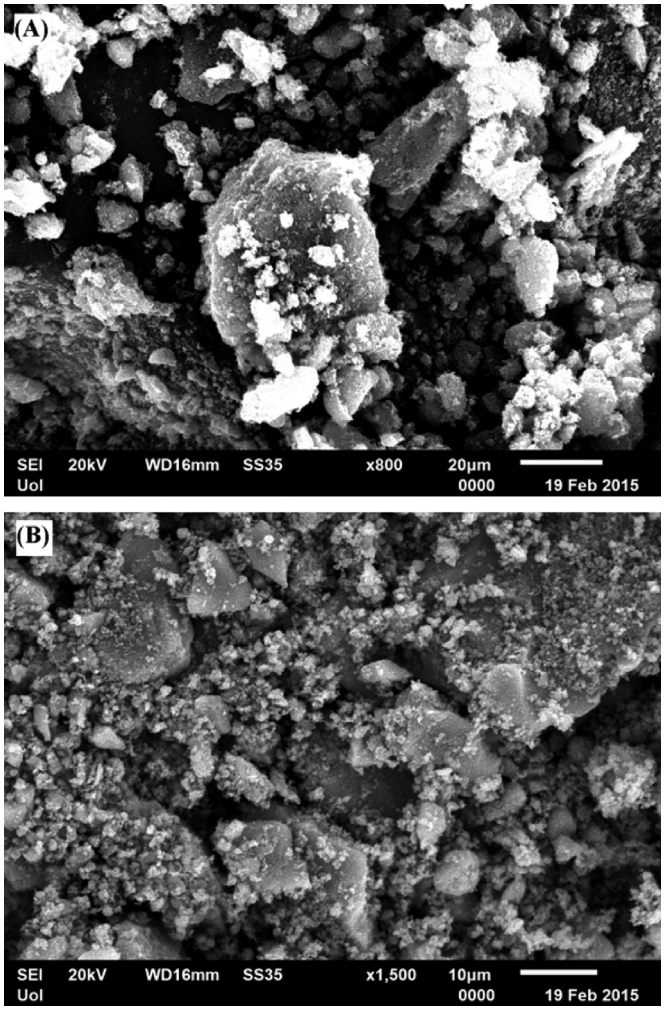

Fig. 3. SEM images of (A) char500 alone, (B) CT0.2/2 PC/TiO_2 composite.

3.2. Surface area and chemistry

Table 1 lists, the BET surface area (S_{BET}) for each PC/TiO_2 composite catalyst. The surface area of pyrolytic tire char calcined at 500 °C was 135 m^2 g^{-1}. For PC/TiO_2 nanocomposites the surface areas are proportional to the amount of pyrolytic char in the catalysts. For example for PC/TiO_2 = 0.1, SSA = 44 m^2 g^{-1} while for PC/TiO2 = 1/2, SSA = 127 m^2 g^{-1}. Also, the point of zero charge (pH_{pzc}) for the PC catalysts and TiO_2 blank are shown in Table 1. We observe that at increasing PC/TiO_2 ratio, the PZC values are more acidic. This shows that PC/TiO_2 composites after calcination at 500 °C retain more acidic groups, carboxylates, as corroborated by the FT-IR spectra.

FT-IR spectra of pyrolytic char/TiO_2 composite catalysts are presented in Fig. 4. The broad band around 3743 cm^{-1} is assigned to the —OH stretching vibration due to surface hydroxyl groups and chemisorbed water on the TiO_2 surface, respectively. The band at 1610 cm^{-1} corresponded to water adsorbed vibrations or stretching vibration of carbonyl groups from carboxylate groups [33]. The band at 2346 cm^{-1} is due to CO_2 in the photometer chamber. The peak at 1098 cm^{-1} is assigned to the C—O vibration in alcohol or quinonic groups [34]. The absorption peak at 670 cm^{-1} corresponds to Ti—O bond vibrations in the TiO_2 [35].

3.3. UV–vis DRS measurements

The UV–vis DRS spectra of the PC/TiO_2 catalysts are presented in Fig. 2. All PC/TiO_2 composites show an intense absorption in the

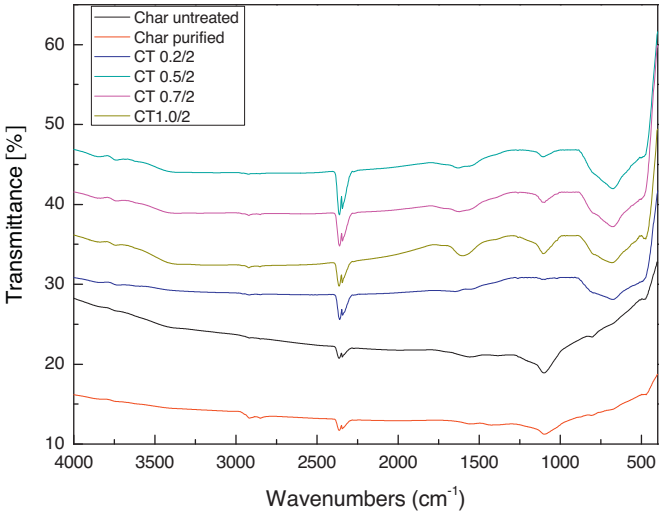

Fig. 4. FTIR spectra of pyrolytic tire char (untreated and purified) and PC/TiO_2 nanocomposites catalysts.

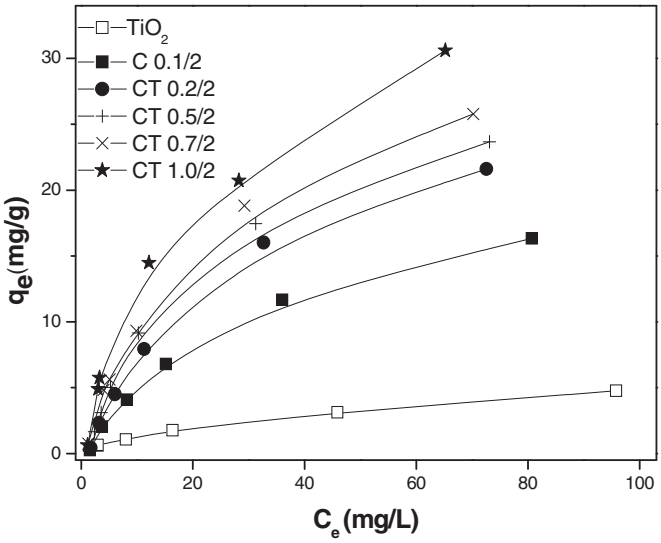

Fig. 5. Equilibrium adsorption isotherms of phenol on pyrolytic tire char and TiO_2.

Table 2
Elemental analysis of pyrolytic char and PC composite catalysts.

Code name	%C	%N	%H	%S	%O[a]	H/C	O/C	(O+N)/C
$Char_{(asreceived)}$	72.53	4.76	4.70	2.84	15.17	0.07	0.21	0.28
$Char_{500}$	66.03	3.55	3.19	0.09	27.23	0.05	0.41	0.47
CT 1/2	15.68	1.25	1.45	0	81.90	0.09	5.22	5.30
CT 0.7/2	11.68	0.97	0.93	0	86.14	0.08	7.37	7.45
CT 0.5/2	5.09	0.90	0.68	0	93.33	0.13	18.34	18.52
CT 0.2/2	2.13	0.79	0.44	0	96.64	0.20	45.37	45.75
CT 0.1/2	1.04	0.35	0.32	0	98.29	0.30	94.51	94.85

[a] Oxygen content determined by difference.

UV region of the spectra, which is due to promotion of e^- from the valence band to the conduction band of TiO_2 [23]. The presence of pyrolytic tire char enhances the visible spectral absorbance in the range of 420–800 nm e.g., as manifested by the upshift of the absorbance spectrum at increasing PC/TiO_2 ratio, see Fig. 2. Thus, absorption in the visible region increased as the amount of pyrolytic char in the catalysts also increased. Band-gap energies, E_g, for PC/TiO_2 photocatalysts were calculated by plotting the transformed Kubelka–Munk function versus the irradiation energy as shown in Fig. 2S (Supplementary information). The calculated E_g values are listed in Table 1.

3.4. Elemental analysis

The results of elemental composition of pyrolytic char calcined at 500 °C, untreated and PC/TiO_2 composite catalysts are summarized in Table 2. As can be seen from the values of carbon content, the C-content increased by 3.5%, 7%, 15%, 16% and 17% for the CT 0.1/2, CT 0.2/2, CT 0.5/2, CT 0.7/2 and CT 1.0/2, respectively.

3.5. Adsorption studies

In order to explain the phenol adsorption process, pseudo first-order, pseudo second order, intraparticle diffusion and Elovich kinetic models were used to fit the experimental data (data not shown). The equilibrium time was found to be 60 min. The determined q_e values calculated from pseudo-second order kinetics are in good agreement with the experimental values of q_e, the calculated correlation coefficients (R^2) are ~1 and the sum of the squares of the errors (SSE) were low, while the other tested models presented lower R^2 and higher SSE values. These results indicate that the adsorption of phenol on the pyrolytic tire char follows pseudo-second order kinetics. The pseudo-second order model for adsorption process is controlled probably by chemisorption [36].

Fig. 5 shows the equilibrium isotherms for adsorption of phenol on PC catalysts. The experimental data were fitted with the Langmuir and Freundlich adsorption isotherms to describe the adsorption equilibrium. The adsorption coefficients and correlation coefficients (R^2) obtained from the two models provide important information on the adsorption mechanism and the surface properties of the adsorbent, are listed in Table 3. The Langmuir isotherm has higher correlation coefficient ($R^2 > 0.99$), thus, the Langmuir model provided the best fitting of adsorption data. The adsorbed amount of phenol increases as the pyrolytic char content of the PC composites also increases. This indicates that adsorption occurs mainly on the active sites of the pyrolytic tire char [37].

3.6. Photocatalytic degradation kinetics and recyclability of the catalysts

Photolysis experiments (i.e., without catalyst) were carried out in advance. The removal of phenol after 300 min of irradiation was less than 20%. In Fig. 6 the results of phenol degradation are presented in the two stage-processes: (i) the dark adsorption period and (ii) the UV-induced photocatalytic degradation period. The net photocatalytic removal of phenol during the degradation process by CT 1/2, CT 0.7/2, CT 0.5/2, CT 0.2/2, CT 0.1/2 and TiO_2 blank was 75%, 76%, 90%, 99%, and 65%, respectively. It is clearly demonstrated that the ratio of pyrolytic char to PC largely affected the performance of the composite catalysts and the optimal PC/TiO_2 weight ratio was 0.2/2. On the basis of previous results, as shown in Fig. 3S (Supplementary information) the kinetic photocatalytic degradation rates of phenol can be ascribed to a pseudo-first-order kinetics. Table 4 lists the kinetic parameter's values for the pseudo-first-order model. The apparent first-order rate constant (k_{app}) for photocatalytic degradation of phenol increased from 3.2×10^{-3} min^{-1} to 6.3×10^{-3} min^{-1} with decreasing ratio of PC to TiO_2. Fig. 7 shows a plot of the photocatalytic rate constant (k_{app}) and adsorption equilibrium constant (K_L) of phenol vs the char content in PC/TiO_2 composites. By comparing the dependence of the k_{app} and K_L constants on the PC/TiO_2 ratio, we notice that the apparent first-order rate constant (k_{app}) first increases with increasing PC/TiO_2 ratio, but then decreases. In contrast the phenol adsorption equilibrium constant (K_L) increases with increasing PC/TiO_2 ratio.

Table 3
Adsorption parameters and correlation coefficients (R^2) for Langmuir and Freundlich isotherm models describing the adsorption of phenol on PC composites.

	Freundlich			Langmuir		
Catalyst code name	K_f (mg g^{-1})	1/n (mg L^{-1})	R^2	Q_m (mg g^{-1})	k_L (L mg^{-1})	R^2
TiO_2 blank	0.35	0.57	0.9992	6.94	0.020	0.9802
CT 0.1/2	1.21	0.60	0.9704	24.66	0.024	0.9969
CT 0.2/2	1.65	0.61	0.9614	32.68	0.027	0.9944
CT 0.5/2	2.13	0.57	0.9592	33.26	0.034	0.9959
CT 0.7/2	2.46	0.56	0.9678	36.11	0.036	0.9978
CT 1.0/2	3.12	0.55	0.9719	41.16	0.041	0.9893

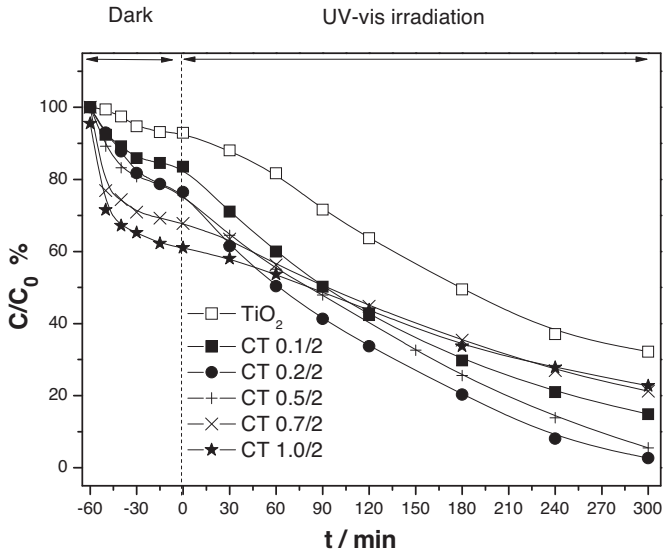

Fig. 6. Combined adsorptive and photocatalytic removal of phenol by the prepared PC/TiO_2 composites and TiO_2 blank catalysts.

Table 4
Apparent first order constant k_{app} (min^{-1}), synergy factor (SF) and correlation coefficients R^2 in the photocatalytic degradation of phenol.

Code name	Apparent removal rate constant, k_{app} (min^{-1})	Synergy factor, (SF)[a]	R^2
Degussa P25	49.3×10^{-3}	–	0.9674
TiO_2 blank	3.2×10^{-3}	1	0.9614
CT0.1/2	5.6×10^{-3}	1.75	0.9996
CT0.2/2	6.3×10^{-3}	1.96	0.9931
CT0.5/2	5.6×10^{-3}	1.75	0.9952
CT0.7/2	3.5×10^{-3}	1.09	0.9857
CT1.0/2	2.8×10^{-3}	0.87	0.9713

[a] SF = {k_{app}(PC/ TiO_2)/k_{app} (TiO_2)} = synergy (SF > 1) or inhibition (SF < 1) factor.

A recycling test was performed to examine the reusability of the best catalyst (CT 0.2/2). It was found that the adsorption capacity after three catalytic cycles remains almost constant and the loss of its photocatalytic activity was negligible (Fig. 4S, Supplementary information).

3.7. EPR study

3.7.1. EPR of h^+/e^- in PC/TiO_2 solids

Fig. 8 presents low-temperature EPR spectra (light-minus-dark at 77 K) for each PC/TiO_2 material in comparison with the TiO_2 blank. In all samples, signals detected at $g = 2.019$, $g = 2.013$ and $g = 2.004$ are due to photoinduced Ti^{4+}—O•—Ti^{4+}—OH states that correspond to trapped holes (h^+) [38,39]. The signals detected at $g = 1.996$ and $g = 1.957$ correspond to electron-trapping Ti^{3+} sites.

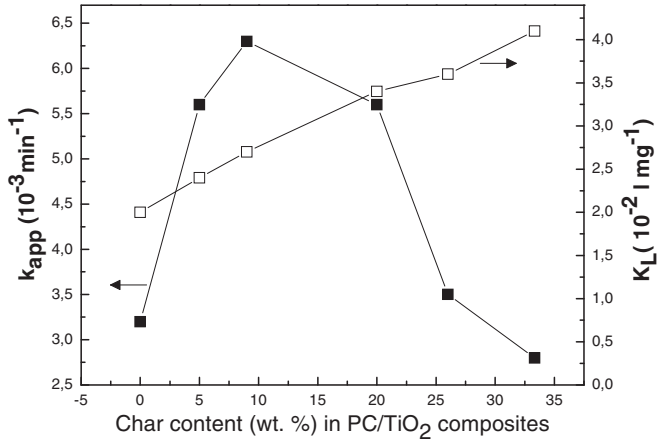

Fig. 7. Rate constant (k_{app}) of phenol photocatalytic degradation and the adsorption equilibrium constant (K_L) as a function of the char content in the composite catalysts PC/TiO_2.

More specifically the signal at $g = 1.996$ corresponds to photoinduced Ti^{3+} electrons into the TiO_2 crystal lattice while the broad signal at $g = 1.957$ corresponds to surface electrons trapped on the TiO_2 particle surface [38,39]. The dynamics of these h^+ and e^- -trapping sites were probed using Cr(VI) as an efficient electron scavenger and isopropanol as a hole scavenger. As shown in Fig. 8 (blue lines) the intensity of the holes' signal increased in the presence of the electron acceptor Cr(VI). On the other hand, in the presence of isopropanol (red lines in Fig. 8) the h^+-signal decreased. This was accompanied by formation of a new four-line signal (intensity ratio 1:3:3:1 at $g \sim 2.0035$) that is typical of methyl radicals formed upon oxidation of isopropanol from the photoinduced holes [39]. These experimental results confirm that the h^+-signal in all cases is related to the surface hydroxyl group as stated above.

When we compare the trends for the holes/electrons in the PC/TiO_2 materials (Fig. 8) we notice that: in CT 0.2/2 the intensity of the holes' (h^+) signal (Fig. 8b) is 25% higher than in TiO_2 blank (Fig. 8f). In comparison with the other PC/TiO_2 composites, the [CT 0.2/2] h^+ signal is 25% higher than [CT 0.1/2] (Fig. 8a), 30% greater than [CT 0.7/2] (Fig. 8c), 50% greater than [CT 0.7/2] (Fig. 8d) and 75% greater than [CT 1/2] (Fig. 8e). Importantly, in all PC/TiO_2 photocatalysts the electron signals are characteristically smaller than the signals of TiO_2 blank (Fig. 8f). Even under isopropanol (see red lines in Fig. 8) the e^--signals don't change notably. On the other hand, the reduction of Cr(VI) to Cr(V) (see blue lines in Fig. 8) proves that there is significant photogeneration of electrons in the PC/TiO_2 composites. Thus, we conclude that, in PC/TiO_2 the carbon matrix acts as an electron-sink i.e., taking up electrons from the TiO_2 particles. In the presence of a strong electron acceptor e.g., such as Cr(VI), electrons moving from the carbon-matrix to the Cr(VI) reducing them rapidly to Cr(V).

Finally, it is worth noting also that carbon doping of the anatase phase did not occur, since we have not detected the corresponding

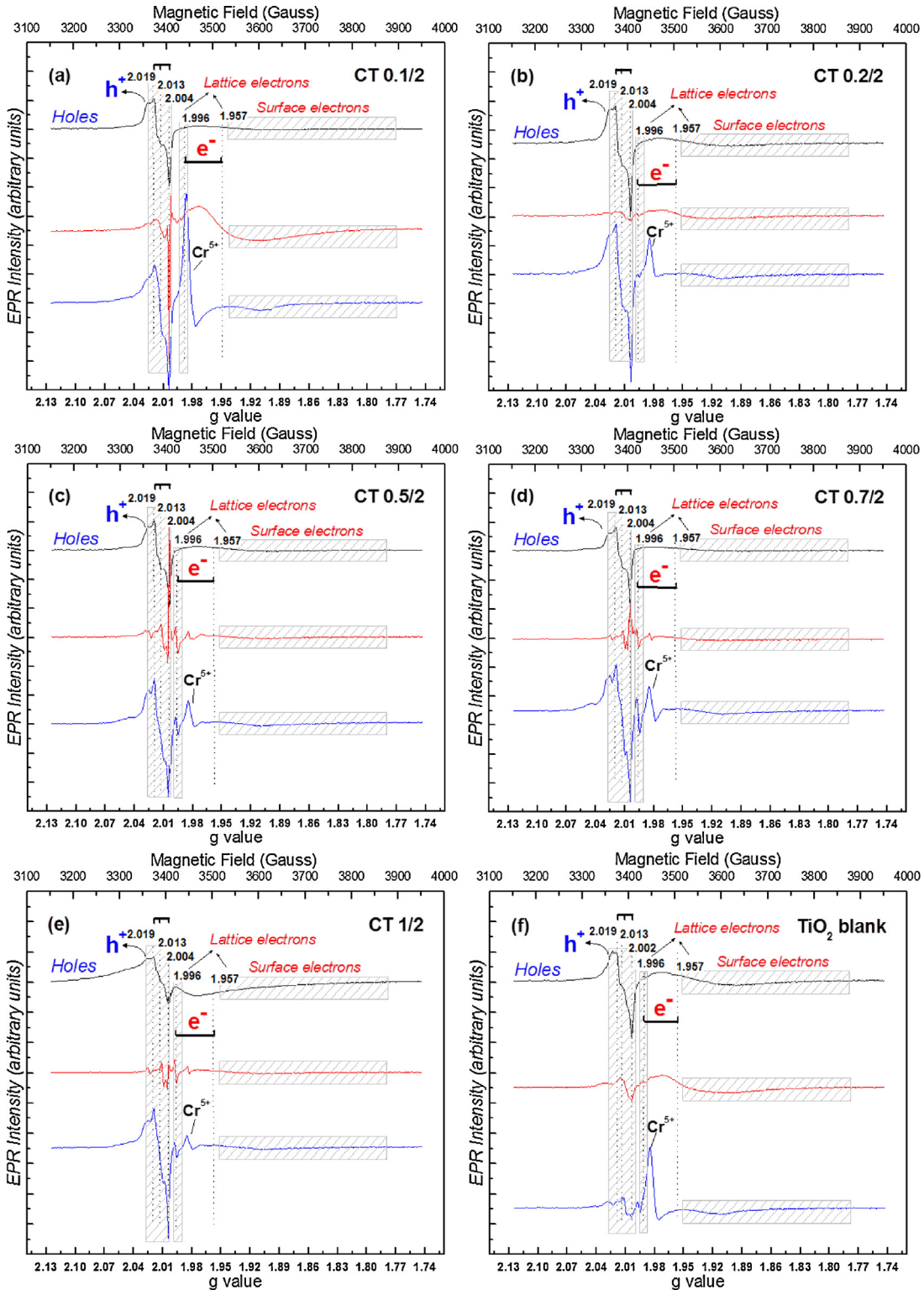

Fig. 8. Light-minus-Dark EPR spectra for (a) CT 0.1/2 (b) CT 0.2/2 (c) CT 0.5/2 (d) CT 0.7/2 (e) CT 1/2 and (f) TiO_2 blank recorded at 77 K with continuous UV–vis irradiation. Black line: powder sample. Red line: under isopropanol vapor. Blue line: in presence of Cr(VI) [05 mM] solution in water (pH 2). (For interpretation of the references to color in this figure legend, the reader is referred to the web version of this article.)

broad signals around $g \sim 2.003$ and we did not observe enhancement of the photocatalytic activity under visible light irradiation [40]. Additional, in all PC/TiO_2 photocatalysts the optical absorption edge remaining around 3.2 eV (see Table 1) compared to the C-doped materials in the literature where there is a shift in the band gap by 0.5 eV (2.7 eV) [40].

Thus, the EPR data reveal that (i) incorporation of TiO_2 on pyrolytic carbon matrix affects severely the populations of the photo-induced hole/electron pairs, and (ii) there is a loss of electrons from the TiO_2 crystal and simultaneous accumulation of holes (h^+). The pyrolytic carbon matrix acts as a sink for the photo-induced electrons which migrate from the TiO_2 crystal into the PC

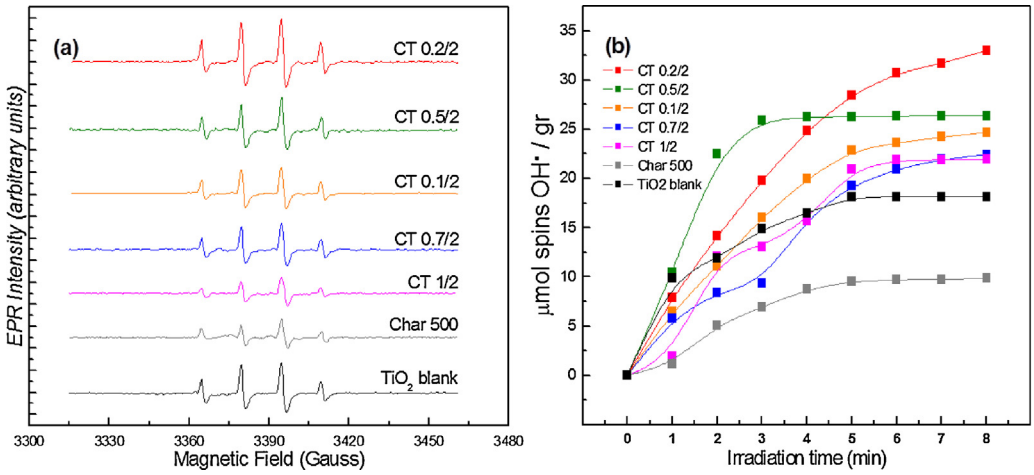

Fig. 9. (a) EPR spectra for the photo-induced •OH radicals of each PC/TiO_2 material in presence of aqueous DMPO [25 mM] at room temperature. Hyperfine splitting correspond to $A_x = A_y = A_z = 15$G. (b) [DMPO-OH] vs time kinetics for the EPR signals of each photocatalytic material.

matrix. This resulted in an increased h^+ lifetime e.g. as evidence from their enhanced EPR spectra, due to diminished hole–electron recombination. Consequently, PC matrix can act as an electron storage matrix for photo-induced electrons from TiO_2. An analogous phenomenon has been documented for grapheme oxide/TiO_2 nanocomposites [41] where GO can behave as an electron storage matrix. Here, it is shown – for the first time to our knowledge – that low-cost pyrolytic carbon is capable to act as an electron storage matrix. These trapped electrons absorb broadly in the red part of the visible spectrum [40] and thus, transforms the gray-black color of an initial aquatic suspension of CT0.5/2 sample into blue–gray color after 9 h visible irradiation as shown clearly in Fig. 5S (Supplementary information).

3.7.2. EPR of OH-radicals in solution

Our DMPO-OH spin-trapping experiments demonstrate that all PC/TiO_2 photocatalysts produced significant amounts of •OH radicals (Fig. 9). The CT 0.2/2 photocatalyst is the one with the highest yield (35 μmol •OH/g). It should be noted that char500 has an OH—yield of 10 μmol •OH/g while TiO_2 blank had 17 μmol •OH/g.

The EPR data in Fig. 9 show that incorporation of TiO_2 onto PC results in two beneficial effects: (i) enhanced OH—production yield, (ii) faster photo-kinetics of •OH generation in solution. Both these beneficial phenomena in solution can be attributed to the enhanced h^+ generation in the TiO_2 crystal e.g., that ultimately is due to the e^-storage ability of the PC matrix that diminishes the h^+/e^- recombination.

3.8. Photocatalytic process and mechanism

Fig. 7 shows a correlation between the apparent first-order rate constants versus PC-content of the studied composites. It is clearly evidenced that the rate constant first increases, with increasing the PC-content from 0.1 to 0.2 g, but then decreases. The highest rate constant ($k_{app} = 6.3 \times 10^{-3}$ min^{-1}) was obtained for 9% wt. char content (0.2/2 ratio). A synergy factor (SF) has been calculated by the ratio of kinetic constants for PC/TiO_2 vs pure TiO_2 in order to quantify the extent of the synergy for the composite catalysts [15]. The so-calculated SF values are listed in Table 4. Among the PC/TiO_2 composite photocatalysts, CT 0.2/2 showed the highest SF value, followed by CT 0.5/2 and CT 0.7/2, except for the case of CT 1.0/2 i.e., the catalyst with the highest char content which inhibited titania's photoactivity by a SF = 0.87. The relative coverage of pyrolytic char by the TiO_2 particles decreases in that case, thus, the average diffusion length of adsorbed phenol toward TiO_2 is increasing with decreasing the TiO_2 percent [19]. Moreover, an increase in the fraction of char inhibits photon uptake by the TiO_2 surface thus decreasing in this way the effective photocatalytic activity of TiO_2 [18].

The enhancement of the photocatalytic rates for the PC/TiO_2 composites compared to neat TiO_2 up to a ratio PC/TiO_2 0.7/2 might be attributed to the well dispersed TiO_2 particles on the surface of PC as revealed by XRD pattern (Fig. 1), since the phenol adsorbed on the surface of pyrolytic char can be easily transferred to the surface of TiO_2. However, the photodegradation rate of phenol increases with decreasing the fraction of pyrolytic char in the composite catalyst up to 0.2/2 ratio, then decreasing for the lower ratios. This indicates that photocatalytic rates do not follow monotonically the adsorption capacities of PC composite catalysts.

Our EPR results indicate that the generation of positive holes in TiO_2 and consequently the production of •OH radicals are improved in the presence of pyrolytic char because of the electron transfer from the conduction band of TiO_2 particles to the graphitic structure of pyrolytic char which reduce the recombination of electrons–holes in TiO_2. This is in good agreement with a recent study [18] regarding the degradation of organic pollutants in the liquid phase using TiO_2/carbon black composite catalysts as reported by Mao's group [18]. They also observed an analogous enhancement of photocatalytic activity of TiO_2 incorporated with carbon black [18].

Overall, the present data show that the efficiency of the catalysts for different PC/TiO_2 ratios is governed by synergistic action of the following mechanism: (i) enhanced adsorption of phenol due to the presence of char and the diffusion of the adsorbed phenol from char toward TiO_2, (ii) enhanced •OH production in solution due to decreased electron–hole pair recombination rates in TiO_2 thanks to the "e-sink" effect of the PC matrix, iii) at increasing PC content, the "filter effect" of the pyrolytic char toward light penetration into the solution decreasing the photo-excitation of TiO_2.

4. Conclusions

The present work investigates the effect of titania (TiO_2) incorporated on tire rubber pyrolytic char (PC) on its performance for photocatalytic degradation of phenol in aqueous solutions. Sol–gel method has been successfully used to prepare PC/TiO_2 nanocomposites catalysts. XRD showed anatase TiO_2 crystal phase for all composite catalysts. The surface area of the catalysts, ranged to SSA = 44.0 – 127.2 $m^2 g^{-1}$ for the PC/TiO_2 0.1/2–1.0/2 e.g., SSA increased proportionally to the amount of char in PC/TiO_2.

The maximum adsorption of phenol ranged from 24.7 mg g^{-1} to 41.2 mg g^{-1} for PC/TiO_2 0.1/2–1.0/2, following the Langmuir isotherm model. The degradation of phenol followed a pseudo-first order kinetic model. The nanocomposite catalysts PC/TiO_2 exhibited an improved photocatalytic activity for degradation of phenol in comparison with pure-TiO_2, in aqueous solutions. CT 0.2/2 catalyst showed the highest photocatalytic degradation and a synergy effect factor SF of 1.96. The enhancement of photocatalytic activity of TiO_2 might be attributed to the increased adsorption of phenol on char, the better dispersion of TiO_2 on the char surface and the electron-storage capacity of PC which can decrease the electron–hole recombination rate of photo-generated in TiO_2.

Acknowledgments

This work is financially supported by the "SYNERGASIA" Program 11SYN_5_682 (O.P. Competitiveness & Entrepreneurship (EPAN II), ROP Macedonia- Thrace, ROP Crete and Aegean Islands, ROP Thessaly- Mainland Greece- Epirus, ROP Attica.

Appendix A. Supplementary data

Supplementary data associated with this article can be found, in the online version, at http://dx.doi.org/10.1016/j.apcatb.2015.03.007.

References

[1] V. Vimonses, B. Jin, C.W.K. Chow, C. Saint, Water Res. 44 (2010) 5385–5397.
[2] P.V. Kamat, D. Meisel, Semiconductor Nanoclusters – Physical, Chemical, and Catalytic Aspects, Elsevier Inc., New York, 1996.
[3] J.W. Park, Y. Kim, H.S. Seon, K.S. Kim, D.W. Park, Thin Solid Films 518 (2010) 4113–4116.
[4] A. Fujishima, T.N. Rao, D.A. Tryk, J. Photochem. Photobiol. C: Photochem. Rev. 1 (2000) 1–21.
[5] A. Zaleska, Rec. Pat. Eng. 2 (2008) 157–164.
[6] L.G. Devil, R. Kavitha, Appl. Catal. B: Environ. 140–141 (2013) 559–587.
[7] T. Torimoto, S. Ito, S. Kuwabata, H. Yoneyama, Environ. Sci. Technol. 30 (1996) 1275–1281.
[8] N. Takeda, M. Ohtani, T. Torimoto, S. Kuwabata, H. Yoneyama, J. Phys. Chem. B 101 (1997) 2644–2649.
[9] G. Colon, M.C. Hidalgo, M. Macias, J.A. Navio, J.M. Dona, Appl. Catal. B: Environ. 43 (2003) 163–173.
[10] B. Tryba, A.W. Morawski, M. Inagaki, Appl. Catal. B: Environ. 41 (2003) 427–433.
[11] W. Wang, C.G. Silva, J.L. Faria, Appl. Catal. B: Environ. 70 (2007) 470–478.
[12] M. Janus, M. Inagaki, B. Tryba, M. Toyoda, A.W. Morawski, Appl. Catal. B: Environ. 63 (2006) 272–276.
[13] A.K. Subramani, K. Byrappa, S. Ananda, K.M. LokanathaRai, C. Ranganathaiah, M. Yoshimura, Bull. Mater. Sci. 30 (2007) 37–41.
[14] B. Tryba, A.W. Morawski, M. Inagaki, Appl. Catal. B: Environ. 46 (2003) 203–208.
[15] J. Matos, J. Laine, J.M. Hermann, Appl. Catal. B: Environ. 118 (1998) 281–291.
[16] N. Takeda, T. Torimoto, S. Sampath, S. Kuwabata, H. Yoneyama, J. Phys. Chem. 99 (1995) 9986–9991.
[17] L.S. Li, W.P. Zhu, P.Y. Zhang, Z.Y. Chen, W.Y. Han, Water Res. 37 (2003) 3646–3651.
[18] C.C. Mao, H.S. Weng, Chem. Eng. J. 155 (2009) 744–749.
[19] N. Takeda, N. Iwata, T. Torimoto, H. Yoneyama, J. Catal. 177 (1998) 240–246.
[20] G.S. Miguel, G.D. Fowler, C.J. Sollars, Ind. Eng. Chem. Res. 37 (1998) 2430–2435.
[21] M.E. Rincon, M.E. Trujillo-Camocho, A.K. Cuentas-Gallegos, Catal. Today. 107–108 (2005) 606–611.
[22] M.E. Rincon, M.E. Trujillo-Camocho, A.K. Cuentas-Gallegos, N. Casillas, Appl. Catal. B: Environ. 69 (2006) 65–74.
[23] M.E. Rincon, M.E. Trujillo, J. Avalos, N. Casillas, J. Solid State Electrochem. 11 (2007) 1287–1294.
[24] Y.J. Xu, Y. Zhuang, X. Fu, J. Phys. Chem. C. 114 (2010) 2669–2676.
[25] J.S. Noh, J.A. Schwarz, J. Colloid Interf. Sci. 130 (1989) 157–164.
[26] K. Bourikas, J. Vakros, C. Kordulis, A. Lycourghiotis, J. Phys. Chem. B 107 (2003) 9441–9451.
[27] G. Grigoropoulou, K.C. Christoforidis, M. Louloudi, Y. Deligiannakis, Langmuir 23 (2007) 10407–10418.
[28] C.D. Jaeger, A. Bard, J. Phys. Chem. 83 (1979) 3146–3152.
[29] N.D. Yordanov, A. Christova, Appl. Magn. Reson. 6 (1994) 341–345.
[30] M.A. Grela, M.E.J. Coronel, A.J. Colussi, J. Phys. Chem. 100 (1996) 16940–16946.
[31] H.M. Rietveld, Acta Crystallogr. 22 (1967) 151–152.
[32] B. Gao, P.S. Yap, T.M. Lim, T.T. Lim, J. Chem. Eng. 171 (2011) 1098–1107.
[33] C.I. Sainz-Diaz, A.J. Griffiths, Fuel 79 (2000) 1863–1871.
[34] J. Yang, K. Qiu, Environ. Sci. Technol. 43 (2009) 3385–3390.
[35] V. Djokić, A. Marinković, O. Ersen, P. Uskoković, R. Petrović, V. Radmilović, D. Janaćković, Ceram. Int. 40 (2014) 4009–4018.
[36] F. Tan, D. Sun, J. Gao, Q. Zhao, X. Wang, F. Teng, X. Quan, J. Chem. J. Hazard. Mater. 244–245 (2013) 750–757.
[37] I. Langmuir, J. Am. Chem. Soc. 40 (1918) 1361–1403.
[38] R.F. Howe, M. Gratzel, J. Phys. Chem. 91 (1987) 3906–3909.
[39] Y. Nakaoka, Y. Nosaka, J. Photochem. Photobiol. A: Chem. 110 (1997) 299–305.
[40] G. Liu, C. Han, M. Pelaez, D. Zhu, S. Liao, V. Likodimos, N. Ioannidis, A.G. Kontos, P. Falaras, P.S.M. Dunlop, J.A. Byrne, D.D. Dionysiou, Nanotechnology 23 (2012) 294003.
[41] G. Williams, B. Seger, P.V. Kamat, ACS Nano 2 (2008) 1487–1491.